

**Dynamically Reconfigurable Bipolar Optical Gradient Force Induced by Mid-Infrared Graphene Plasmonic Tweezers for Sorting Dispersive Nanoscale Objects***Puspita Paul, and Peter Q. Liu\**

P. Paul, Prof. P. Q. Liu  
Department of Electrical Engineering, University at Buffalo, The State University of New York, Buffalo, NY 14260, United States  
E-mail: pqliu@buffalo.edu

**Keywords:** graphene plasmonics, optical tweezers, nanoparticle sorting and fractionation, mid-infrared, repulsive gradient force

**Abstract**

Existing techniques for optical trapping and manipulation of microscopic objects, such as optical tweezers and plasmonic tweezers, are mostly based on visible and near-infrared light sources. As it is in general more difficult to confine light to a specific length scale at a longer wavelength, these optical trapping and manipulation techniques have not been extended to the mid-infrared spectral region or beyond. Here, we show that by taking advantage of the fact that many materials have large permittivity dispersions in the mid-infrared region, optical trapping and manipulation using mid-infrared excitation can achieve additional functionalities and benefits compared to the existing techniques in the visible and near-infrared regions. In particular, we demonstrate that by exploiting the exceedingly high field confinement and large frequency tunability of mid-infrared graphene plasmonics, high-performance and versatile mid-infrared plasmonic tweezers can be realized to selectively trap or repel nanoscale objects of different materials in a dynamically reconfigurable way. This new technique can be utilized for sorting, filtering and fractionating nanoscale objects in a mixture.

## 1. Introduction

Since the invention of optical tweezers several decades ago,<sup>[1,2]</sup> a variety of optical trapping techniques have been developed for manipulating microscopic objects.<sup>[3-6]</sup> The more recent development of plasmonic tweezers further improves the optical trapping performance by exploiting the large near-field confinement of plasmonic structures,<sup>[7-13]</sup> which overcomes the diffraction limit constraining the ultimate trapping capability of conventional optical tweezers. Trapping of various types of objects including dielectric<sup>[7]</sup> and metallic<sup>[8]</sup> nanoscale particles, large biomolecules,<sup>[9,10]</sup> and quantum dots<sup>[11]</sup> with sizes down to a few nm has been demonstrated using different metallic plasmonic structures, such as dipole antennas and nano-apertures. However, there are also major limitations associated with plasmonic tweezers based on metals. Metallic plasmonic structures lack real-time tunability, which makes it relatively complicated to dynamically tune the induced optical force for versatile manipulation of trapped objects, such as precise transportation and displacement.<sup>[12-14]</sup> Furthermore, most of the metallic plasmonic tweezers (and conventional optical tweezers) operate using visible or near-infrared (NIR) excitation sources. Such excitation sources with relatively high photon energies may cause undesired change or damage to sensitive objects (e.g., biological organisms or biomolecules) that are optically trapped, or induce optical signals (e.g., photoluminescence or fluorescence) that interfere with the observation of trapped objects. These issues can be avoided by realizing optical trapping and manipulation in a spectral region of lower photon energy, such as the mid-infrared (MIR). Therefore, employing MIR plasmonic structures with real-time tunability is an effective way to address these aforementioned limitations of metallic plasmonic tweezers and further expand the range of techniques for optical trapping and manipulation, which may lead to new functionalities and applications. Moreover, optical forces induced by MIR excitations can also be combined with various infrared spectroscopy techniques to probe chemical-specific information of characterized samples. For example, in recent years, photo-induced force microscopy techniques employing MIR excitations have been developed to

obtain high-resolution spatial maps of the chemical compositions of heterogeneous materials and nanoscale objects.<sup>[15-17]</sup>

During the past decade, graphene has emerged as one of the most appealing materials for tunable MIR plasmonics.<sup>[18-22]</sup> Graphene plasmonic resonances in the MIR region typically have exceedingly high (about two orders of magnitude) field confinement and enhancement, which effectively overcomes the disadvantage of relatively longer wavelengths of MIR light for optical trapping and manipulation. The resonance frequency of a graphene plasmonic structure can be readily tuned across a wide range by changing the graphene carrier density electrically with a gate, which in turn allows for convenient control of the optical force induced by the graphene plasmonic structure. Taking advantage of these favorable properties of graphene plasmonics, several theoretical studies of MIR plasmonic tweezers based on various graphene structures (e.g., ribbons, anti-dots, rings) have been reported in recent years,<sup>[23-27]</sup> which predicted impressive capabilities and performances for trapping and manipulating nanoscale objects. However, all of these previous studies considered the trapped objects as simple dielectric nanoparticles (NPs) with negligible permittivity dispersion. In reality, many materials have polar optical phonons or molecular vibrational modes in the MIR region, which strongly interact with MIR light and lead to large permittivity dispersion that can switch from positive to negative values within a narrow spectral window. Here, we show that such typically large permittivity dispersions of many materials in the MIR region can drastically alter the characteristics of optical forces induced on NPs made of such materials. Specifically, significant reconfigurable bipolar optical force (i.e., trapping or repulsive force) can be induced on NPs with a large material dispersion by tuning the excitation source frequency. A repulsive gradient force occurs when the excitation frequency is within a spectral window which contains the epsilon-near-zero (ENZ) frequency range of the dispersive material. By employing tunable MIR graphene plasmonic structures, we demonstrate new functionalities of optical manipulation of NPs that would be difficult to achieve in the visible and NIR regions. These functionalities can

be utilized to selectively filter, sort and fractionate (separate) NPs in a mixture, and therefore may find a broad range of applications. Our proposed technique takes advantage of the large real-time tunability of graphene plasmonics and the strong permittivity (refractive index) dispersions of many materials in the MIR region, and hence can be more effective and versatile than previously demonstrated optical sorting and fractionating techniques in the visible and NIR regions, which are based on particle size differences and/or comparatively smaller refractive index differences.<sup>[28-33]</sup>

## 2. Results and discussion

### 2.1. Reconfigurable bipolar optical gradient forces induced by MIR graphene plasmonic tweezers on dispersive NPs

In this study, we focus on graphene nanoribbon (GNR) structures for realizing tunable plasmonic trapping and manipulation of NPs, mainly because the GNR geometry allows for convenient formation of plasmonic conveyor belt networks which can be used to trap and manipulate multiple NPs simultaneously and independently,<sup>[26]</sup> although our findings can be applied to any graphene plasmonic structures. The schematic of the investigated GNR plasmonic tweezers is illustrated in **Figure 1a**. A GNR is patterned on a dielectric substrate (refractive index  $n=1.53$  assumed) that also functions as the gate insulator. A 3 nm thick encapsulation layer is added to protect the GNR from the environment (such as a liquid medium). The GNR carrier density (Fermi energy) can be controlled with a back-gate, which in turn determines the GNR plasmonic resonance frequency. The electromagnetic field in the vicinity of the GNR is highly confined and enhanced at its plasmonic resonance, and as a result, a NP in the near field of the GNR can experience a significant optical force. Note that due to the translation invariance of the device structure along the GNR, the optical force does not have a component along the GNR (i.e., y-direction in Fig. 1a), and hence this structure can optically trap a NP in two dimensions (x-direction and z-direction). Nevertheless, three-dimensional

trapping can be achieved by modulating the GNR carrier density distribution along the  $y$ -direction.<sup>26</sup>

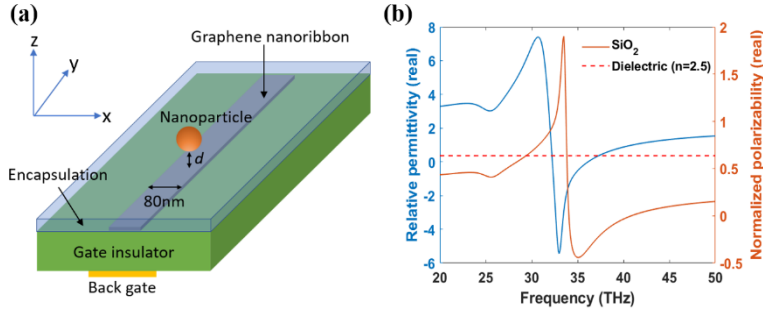


**Figure 1.** (a) Schematic of the investigated GNR plasmonic tweezers for trapping and manipulating NPs. (b) The real part of relative permittivity (solid blue curve) and the real part of normalized polarizability (solid red curve) of a SiO<sub>2</sub> NP. The dashed red line is the normalized polarizability of a dielectric NP with a constant refractive index of  $n=2.5$ . The normalized polarizability (which is also called the Clausius-Mossotti factor) refers to the NP polarizability in Equation (2) divided by the factor  $3\epsilon_0 V$ . The relative permittivity of the surrounding medium is assumed to be  $\epsilon_s = 1$ .

Among different methods for calculating optical force, the dipole approximation provides the most intuitive insight into the influence of a microscopic object's polarizability on the optical force experienced by the object in a non-uniform light field. Within the dipole approximation, the time-averaged total optical force exerted by a monochromatic electromagnetic wave on a dipole-like particle can be expressed as:<sup>[34]</sup>

$$\langle \mathbf{F}(\mathbf{r}) \rangle = \frac{\alpha'}{2} \sum_j \text{Re} \left\{ \left( E_j(\mathbf{r}) \right)^* \nabla E_j(\mathbf{r}) \right\} + \frac{\alpha''}{2} \sum_j \text{Im} \left\{ \left( E_j(\mathbf{r}) \right)^* \nabla E_j(\mathbf{r}) \right\}, \quad (1)$$

where  $\alpha'$  and  $\alpha''$  are the real and the imaginary parts of the particles' complex polarizability  $\alpha$  (i.e.,  $\alpha = \alpha' + i\alpha''$ ),  $j$  stands for  $x, y$  or  $z$ ,  $E_j(\mathbf{r})$  is the  $j$ -component of the complex electric field amplitude at position  $\mathbf{r}$ , and the symbol  $*$  represents complex conjugate. The first term of the above expression is the gradient force component ( $F_{\text{grad}}$ ) associated with the real (dispersive) part of the polarizability and the gradient of the field intensity. The second term defines the

scattering force component ( $F_{\text{scatt}}$ ) which is proportional to the imaginary (dissipative) part of the polarizability. For a spherical NP with a diameter much smaller than the wavelength of light, its complex polarizability can be obtained from the permittivity of the particle's material and that of the surrounding medium according to the Clausius-Mossotti relation:<sup>[34]</sup>

$$\alpha(\omega) = 3\varepsilon_0 V \frac{\varepsilon(\omega) - \varepsilon_s(\omega)}{\varepsilon(\omega) + 2\varepsilon_s(\omega)}, \quad (2)$$

where  $\varepsilon_0$  is the vacuum permittivity,  $V$  is the volume of the NP,  $\varepsilon(\omega)$  and  $\varepsilon_s(\omega)$  define the relative permittivity functions of the NP's material and the surrounding medium, respectively.

Note that the radiation reaction correction to the polarizability is neglected in Equation (2).<sup>[35]</sup>

This is valid when the size of the NP is much smaller than the wavelength of light, which is indeed the case in this study. To conduct optical trapping and manipulation of NPs, usually a medium with negligible loss and hence low dispersion in the spectral range of interest is chosen, and therefore we can assume  $\varepsilon_s$  is a real-valued constant. Some organic solvents such as hexane, decane and several other alkanes have low loss in most of the MIR spectral region, and therefore are suitable liquid media for optical trapping and manipulation employing MIR excitation. The NP's material permittivity is in general complex and dispersive (i.e.,  $\varepsilon(\omega) = \varepsilon'(\omega) + i\varepsilon''(\omega)$ ). According to Equation (2), for a dielectric NP with  $\varepsilon'(\omega) > \varepsilon_s$  or a metallic NP with  $\varepsilon'(\omega) < -2\varepsilon_s$ , the real part of its polarizability  $\alpha'(\omega)$  is positive, which typically leads to a gradient force that tends to trap the NP at the location of the highest light field intensity. This is indeed how optical tweezers and plasmonic tweezers normally operate. However, it is also obvious from Equation (2) that when  $\varepsilon'(\omega)$  is in the range of  $-2\varepsilon_s$  to  $\varepsilon_s$ ,  $\alpha'(\omega)$  can have a negative value (provided that  $\varepsilon''(\omega)$  is not too large), which would in turn lead to a repulsive gradient force if the NP is near the location of the highest field intensity. Such a scenario can occur to metallic NPs in a spectral window not far from the plasma frequency of the metal (usually in the visible and NIR regions).<sup>[6,36-37]</sup> On the other hand, a negative polarizability can also occur to dielectric NPs in the MIR (and terahertz) spectral region, as many dielectric materials exhibit large

permittivity dispersions in the MIR region owing to their polar optical phonons or molecular vibrational modes. Such permittivity dispersions are usually well described by the Lorentz model. Near the frequency of an optical phonon or molecular vibrational mode of a material, the real part of permittivity varies dramatically and can switch its sign, hence satisfying the condition  $-2\varepsilon_s < \varepsilon'(\omega) < \varepsilon_s$  and leading to a negative real part of the NP polarizability. Note that this spectral window for negative NP polarizability also contains the ENZ spectral range of the material (i.e.,  $\varepsilon'(\omega) \approx 0$ ). As an example, **Figure 1b** shows the relative permittivity of silica in the spectral region near its optical phonon mode at  $\sim 33$  THz, and the corresponding normalized polarizability (real part, normalized by  $3\varepsilon_0 V$ ) of a silica sphere which exhibits negative values in the frequency window of  $\sim 34$ – $41$  THz.

To demonstrate the influence of such a strong permittivity (polarizability) dispersion on optical force characteristics, we calculated the optical forces on spherical NPs made of different types of materials using the dipole approximation, which are shown in **Figure 2**. The NPs are assumed to be located at a constant height ( $d=6$  nm) above the GNR (80 nm wide, see Figure 1a). The diameter of the NPs is assumed to be 8 nm in this particular example, since the dipole approximation yields relatively accurate result when the NP size is much smaller than the length scale of the light field confinement. The types of materials considered include a non-dispersive dielectric material (constant refractive index of 2.5), gold, and a dispersive material described by the standard Lorentz model (Lorentz resonance frequency  $f_0=27.7$  THz, static relative permittivity  $\varepsilon_{st}=14$ , high-frequency relative permittivity  $\varepsilon_\infty=10$ , and damping rate  $\Gamma=4\times 10^{12}$  s<sup>-1</sup>). The GNR Fermi energy is set to 0.4 eV, which results in a GNR plasmonic resonance at  $\sim 9.4$   $\mu\text{m}$  ( $\sim 31.8$  THz), corresponding to more than two orders of magnitude of field confinement and enhancement (see **Figure 2a**). Without loss of generality, the surrounding medium is assumed to have a relative permittivity of  $\varepsilon_s = 1$  for all the results shown below, whereas some comparison results obtained at larger relative permittivity values of the surrounding medium are included in the Supporting Information (see **Figure S1**) which show even larger optical

forces owing to the higher field confinement of GNR plasmonic resonance. **Figure 2b** and **2c** show the calculated x-component and z-component, respectively, of the optical force on the Lorentz NP (normalized to the excitation intensity) as a function of the excitation source frequency and the x-coordinate of the NP. Clearly, the optical force on the Lorentz NP switches from a trapping force to a repulsive force as the excitation source frequency varies across 32 THz, i.e., the frequency at which the NP polarizability changes its sign. To illustrate the key difference between the GNR induced optical forces on different types of NPs, **Figure 2d** and **2e** show the calculated x-component and z-component of the x-coordinate-dependent optical forces on the different types of NPs (normalized to the excitation source intensity) at specific excitation source frequencies, and the corresponding potential energy profiles are plotted in **Figure 2f**. When the GNR is excited around its plasmonic resonance, both the non-dispersive dielectric NP and the gold NP experience a significant trapping force in the vicinity of the GNR edges where the field is highly confined. This trapping force reaches its maximum when the GNR is excited exactly at its plasmonic resonance (Figure 2d and 2e). The valleys of the corresponding potential energy profiles are also near the GNR edges (Figure 2f). In contrast, the optical force on the Lorentz NP varies more dramatically near the GNR plasmonic resonance. Slightly below the GNR plasmonic resonance, the polarizability of the Lorentz NP reaches its peak positive value that is larger than those of the dielectric NP and the gold NP, and hence the Lorentz NP experiences a significant trapping force that is also larger than those on the dielectric NP and the gold NP. Slightly above the GNR plasmonic resonance, the polarizability of the Lorentz NP reaches its peak negative value, which leads to a significant repulsive force on the Lorentz NP (Figure 2d and 2e) and a corresponding potential energy barrier (Figure 2f) near the GNR. These calculated optical forces (both trapping and repulsive) are dominated by the gradient force component, which is more than an order of magnitude larger than the scattering force component (see Supporting Information **Figure S2**). To verify the validity of the dipole approximation, we also calculated the optical forces on these NPs

using the Maxwell stress tensor method,<sup>[34]</sup> and the results are shown in Figure 2d-f as the dashed curves, which exhibit good agreement with those obtained using the dipole approximation. Along the z-direction perpendicular to the GNR plane, the amplitude of the z-component of optical force increases monotonically as a NP approaches the GNR (see Supporting Information **Figure S3**), regardless of whether it is a trapping or repulsive force.

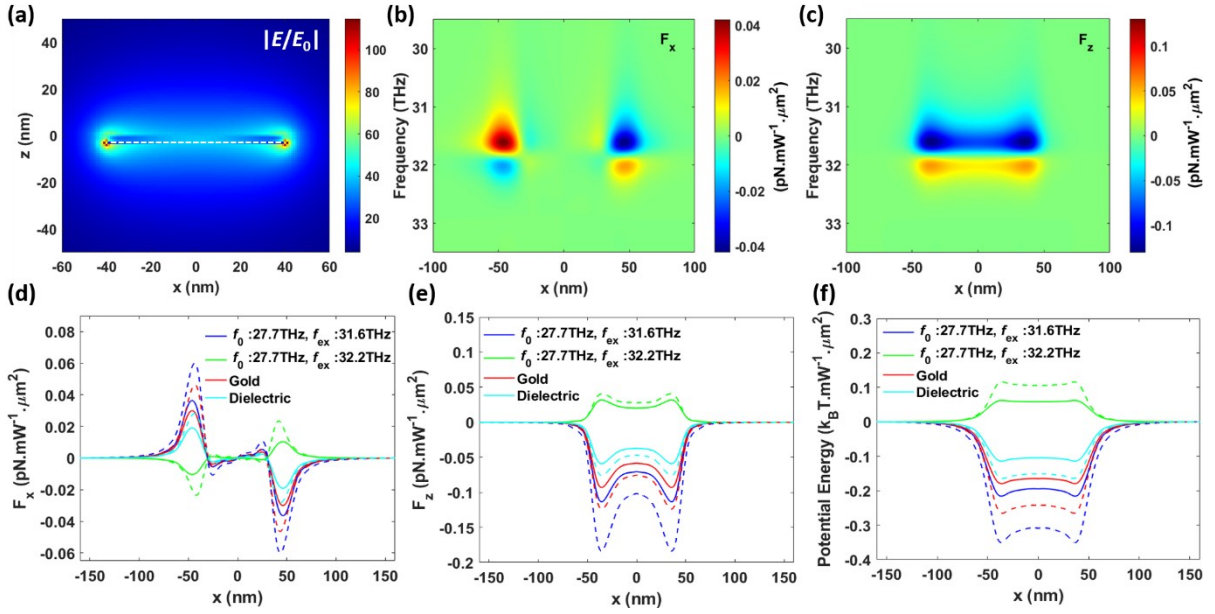


**Figure 2.** (a) Simulated profile of the electric field enhancement in the vicinity of the GNR at its plasmonic resonance. The white dashed line represents the GNR. (b) Calculated x-component  $F_x$  and (c) z-component  $F_z$  of the optical force (normalized to the excitation intensity) on a Lorentz NP (8 nm diameter,  $f_0=27.7$  THz) as a function of the excitation source frequency and the x-coordinate of the NP. The calculation is based on the dipole approximation. The NP is assumed to be at a constant height ( $d=6$  nm) above the GNR as its x-coordinate varies. (d) Calculated x-component  $F_x$  and (e) z-component  $F_z$  of the optical forces (normalized to the excitation intensity) on NPs made of different materials (i.e., non-dispersive dielectric, gold, and the Lorentz model material in (b)-(c)) as functions of the x-coordinates of the NPs at specific excitation source frequencies. For the non-dispersive dielectric NP and the gold NP, the excitation source frequency is the same as the GNR plasmonic resonance frequency ( $\sim 31.8$  THz). For the Lorentz NP, the results at two different excitation source frequencies (i.e.,  $f_{ex}=31.6$  THz and  $f_{ex}=32.2$  THz) near the GNR plasmonic resonance are shown. The solid curves are calculated

using the dipole approximation, and the dashed curves are calculated using the Maxwell stress tensor method. (f) Calculated intensity-normalized potential energy profiles corresponding to the force results in (d).

We further studied the characteristics of optical forces on larger NPs, the sizes of which are comparable to the field confinement length scale. The GNR plasmonic resonance induced optical forces on such larger NPs are calculated using the Maxwell stress tensor method only, since the dipole approximation is no longer accurate in this case. We systematically investigated how the optical force on a Lorentz NP depends on the Lorentz model parameters, such as the Lorentz resonance frequency  $f_0$ , and the results are shown in **Figure 3**. The results on the influence of the other Lorentz model parameters (i.e.,  $\epsilon_{st}$ ,  $\epsilon_{\infty}$ ,  $\Gamma$ ) are included in the Supporting Information (see **Figure S4** to **Figure S6**). **Figure 3a** shows the real part of the normalized polarizability of Lorentz NPs with different Lorentz resonance frequencies ( $f_0$ ) whereas the other model parameters are fixed ( $\epsilon_{st}=14$ ,  $\epsilon_{\infty}=10$ ,  $\Gamma=4\times 10^{12} \text{ s}^{-1}$ ). The normalized polarizabilities of a non-dispersive dielectric NP and a gold NP are also plotted as references. Three of these Lorentz polarizability curves exhibit negative values near the GNR plasmonic resonance (i.e.,  $f_0=26.4 \text{ THz}$ ,  $27 \text{ THz}$  or  $27.7 \text{ THz}$ ), and hence a repulsive gradient force on the corresponding NPs is expected when the system is optically excited near the GNR plasmonic resonance. The spectra of the calculated x-component and z-component of optical forces on the different Lorentz NPs and the reference dielectric and gold NPs are shown in **Figure 3b** and **3c**, respectively. The NPs are assumed to have a diameter of 60 nm and be located at  $d=10 \text{ nm}$  above the GNR edge for these calculations. The excitation source is assumed to be a plane wave with a moderate intensity of  $1 \text{ mW}/\mu\text{m}^2$ , which suggests that, for example, a MIR laser with 1 W power can illuminate a network of multiple GNRs occupying an area of about  $30 \mu\text{m}$  by  $30 \mu\text{m}$ .<sup>[26]</sup> Since the non-dispersive dielectric NP and the gold NP both have positive polarizabilities with negligible dispersion, their optical force spectra closely resemble the

spectrum of the GNR plasmonic resonance. On the other hand, the optical forces on the Lorentz NPs show more complex spectra as a result of the strong polarizability dispersions of these Lorentz NPs. Indeed, the three Lorentz NPs exhibiting negative polarizability values near the GNR plasmonic resonance experience repulsive forces accordingly. As expected, the electromagnetic field profile surrounding the NP when it experiences a repulsive force is also significantly different from that associated with a trapping force (see Supporting Information **Figure S7**). Note that the frequency window in which a Lorentz NP experiences a repulsive force is similar to the frequency window in which the NP has negative polarizability, although they are not exactly the same (which is expected since the dipole approximation is not accurate for NPs of this size). The other three Lorentz NPs (i.e.,  $f_0=23.9$  THz, 29 THz or 30.2 THz) with only positive polarizability values near the GNR plasmonic resonance experience only trapping force within that frequency range. These results indicate that by tuning the excitation source frequency and/or the GNR plasmonic resonance frequency, we can trap or repel a specific type of Lorentz NPs. To more clearly demonstrate this capability, **Figure 3d** and **3e** show the calculated position-dependent x-component and z-component of the optical forces, respectively, on a Lorentz NP with  $f_0=27.7$  THz at two different excitation source frequencies (31.4 THz and 32.3 THz) near the GNR plasmonic resonance, and the corresponding potential energy profiles are shown in **Figure 3f**. At 31.4 THz excitation frequency, the Lorentz NP experiences a significant trapping force with a  $>15k_B T$  potential well depth, which guarantees stable trapping at room temperature. On the other hand, at 32.3 THz excitation frequency, the same Lorentz NP experiences a significant repulsive force which produces a potential barrier of  $\sim 5k_B T$ . Note that for such larger NPs, the lowest (highest) point of the potential well (barrier) is located at the middle of the GNR rather than at the GNR edges (the case for smaller NPs shown in **Figure 2f**), which is a consequence of the difference between the position dependence of optical forces on NPs of different sizes (see **Figure 3d** versus **Figure 2d**).

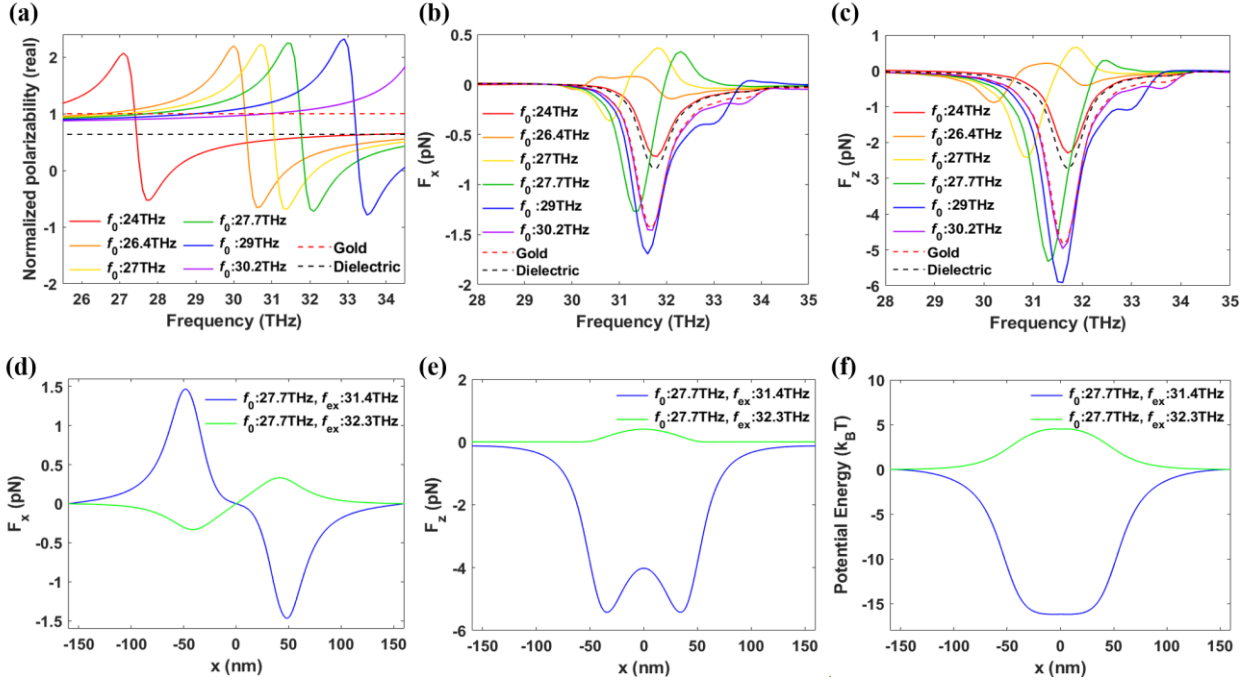


**Figure 3.** (a) Real part of the normalized polarizabilities of different Lorentz NPs with the specified Lorentz resonance frequencies, in comparison with those of a non-dispersive dielectric NP and a gold NP. (b) Calculated x-component ( $F_x$ ) and (c) z-component ( $F_z$ ) of the optical forces as a function of the excitation source frequency, for different Lorentz NPs (60 nm diameter) located at  $d=10$  nm above the GNR edge ( $x=40$  nm), in comparison to those for the dielectric NP and the gold NP of the same size. The GNR plasmonic resonance is at 31.8 THz (graphene  $E_F=0.4$  eV). (d) Calculated x-component and (e) z-component of the optical force on a Lorentz NP ( $f_0=27.7$  THz) at the two specified excitation source frequencies near the GNR plasmonic resonance, as the x-coordinate of the NP varies from -160 nm to 160 nm while the NP height is kept constant at  $d=10$  nm. (f) Calculated potential energy profiles corresponding to the force results in (d).

## 2.2. Potential applications of reconfigurable bipolar optical gradient forces

Such reconfigurable and material-dependent bipolar (trapping or repulsive) optical gradient forces based on MIR excitation sources allow us to select certain types of NPs out of a mixture of multiple different types of NPs. Furthermore, the large electrically-controlled frequency tunability of the GNR plasmonic resonance provides a convenient, versatile and high-performance platform for realizing such selective manipulation of different types of NPs in the

MIR, which can be exploited for various applications such as sorting, filtering and fractionation of nanoscale objects. To conceptually demonstrate the unique functionalities and versatility of this platform, we discuss two exemplary applications here. In the first application example, we consider a mixture of NPs made of two different materials, i.e.,  $\text{Al}_2\text{O}_3$  and  $\text{Fe}_2\text{O}_3$ , which exhibit significantly different permittivity (and hence polarizability) dispersions in the MIR region. As illustrated in **Figure 4a**, by choosing the GNR plasmonic resonance frequency and the excitation source frequency accordingly, we can selectively trap either type of NPs only while repelling the other type, since the two types of NPs exhibit negative polarizability in different frequency windows (see **Figure 4b**). **Figure 4c** and **4d** show the calculated optical forces and potential energy profiles for selectively trapping the  $\text{Al}_2\text{O}_3$  NPs and rejecting the  $\text{Fe}_2\text{O}_3$  NPs. To realize this scenario, the GNR Fermi energy is set to 0.15 eV (corresponding to the GNR plasmonic resonance at 19 THz) and the excitation frequency is at the GNR plasmonic resonance (see Supporting Information **Figure S8** for the optical force spectra). **Figure 4e** and **4f** show the results of the opposite scenario of trapping the  $\text{Fe}_2\text{O}_3$  NPs and rejecting the  $\text{Al}_2\text{O}_3$  NPs, with the GNR Fermi energy set at 0.3 eV and the excitation frequency at 27.4 THz (i.e., the GNR plasmonic resonance). In either scenario, the depth of the trapping potential well exceeds  $10k_{\text{B}}T$ , and the potential barrier for the rejected NPs is also significant (more than  $5k_{\text{B}}T$ ), which may adequately prevent collisions of the two types of NPs due to their Brownian motions. In addition to these two scenarios, both types of NPs can be trapped simultaneously by shifting the GNR plasmonic resonance and the excitation frequency to a range in which both NPs have positive polarizabilities (not shown in Figure 4).

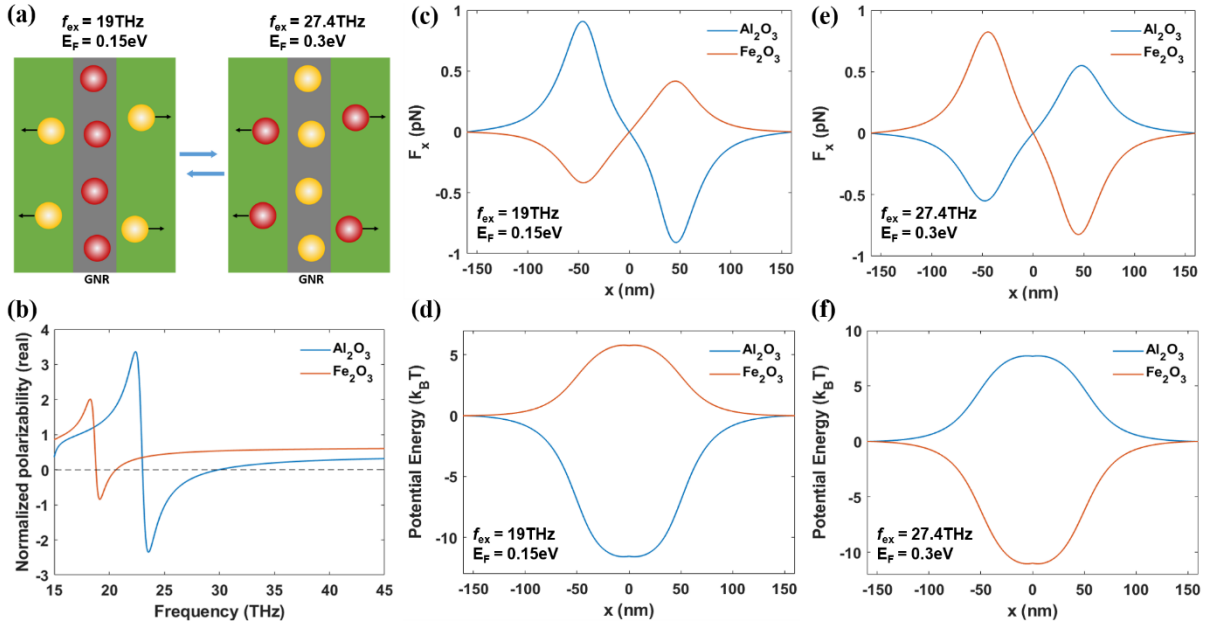


**Figure 4.** NP sorting and fractionating functionality I. (a) Conceptual schematic illustrating the functionality of selectively trapping one type of NPs while rejecting the other type in a mixture, by tuning the GNR Fermi energy (and hence plasmonic resonance) and the excitation source frequency accordingly. (b) The normalized polarizabilities of Al<sub>2</sub>O<sub>3</sub> NPs and Fe<sub>2</sub>O<sub>3</sub> NPs in part of the MIR spectral region. (c) Calculated x-component ( $F_x$ ) of the GNR-induced optical forces on the two types of NPs, and (d) the corresponding potential energy profiles, at the GNR Fermi energy  $E_F=0.15$  eV and the excitation source frequency  $f_{ex}=19$  THz. In this operating condition, the Al<sub>2</sub>O<sub>3</sub> NPs are trapped whereas the Fe<sub>2</sub>O<sub>3</sub> NPs are repelled by the GNR. (e) Calculated x-component ( $F_x$ ) of the optical forces on the two types of NPs, and (f) the corresponding potential energy profiles, at the GNR Fermi energy  $E_F=0.3$  eV and the excitation source frequency  $f_{ex}=27.4$  THz. In this operating condition, the Fe<sub>2</sub>O<sub>3</sub> NPs are trapped whereas the Al<sub>2</sub>O<sub>3</sub> NPs are repelled by the GNR. A moderate excitation source intensity at  $1.5$  mW/ $\mu\text{m}^2$  is assumed for calculating the results in this figure.

In the second application example, we consider a single type of dispersive NPs made of Al<sub>2</sub>O<sub>3</sub>, with a percentage of which coated with a thin dielectric layer and hence forming a core/shell NP structure. This scenario may well represent certain biomolecular studies which involve attaching biomolecules (e.g., protein, antibodies, DNAs) to various types of NPs. Such a core/shell NP can exhibit an equivalent polarizability that is considerably different from that of

the core NP<sup>[38]</sup> (see Supporting Information **Figure S9**). Therefore, as illustrated in **Figure 5a**, we can tune the GNR plasmonic resonance and the excitation source frequency accordingly to either selectively trap the coated NPs while rejecting the uncoated NPs, or vice versa. **Figure 5b** plots the normalized polarizability of an uncoated Al<sub>2</sub>O<sub>3</sub> NP and that of the same Al<sub>2</sub>O<sub>3</sub> NP with a 4 nm thick dielectric coating ( $n=2.5$ ). We can clearly see that a key difference between the two polarizability functions is that the dielectric-coated Al<sub>2</sub>O<sub>3</sub> NP exhibits negative polarizability in a lower frequency window than the uncoated Al<sub>2</sub>O<sub>3</sub> NP. **Figure 5c** and **5d** show the calculated optical forces and the corresponding potential energy profiles for the first scenario in Figure 5a, in which only the coated Al<sub>2</sub>O<sub>3</sub> NPs are trapped by the GNR and the uncoated Al<sub>2</sub>O<sub>3</sub> NPs are rejected. **Figure 5e** and **5f** show the results for the second scenario, in which only the uncoated Al<sub>2</sub>O<sub>3</sub> NPs are trapped and the coated Al<sub>2</sub>O<sub>3</sub> NPs are rejected (see Supporting Information **Figure S10** for the optical force spectra). In both scenarios, the GNR plasmonic resonance and the excitation source frequency are chosen to optimize the trapping potential depths. By further adjusting the operating condition, trapping both coated and uncoated NPs can also be achieved (not shown in Figure 5). In principle, given any type of material (with or without dispersion) of the thin coating, the material of the NPs can be meticulously chosen to optimize the selective trapping performance, such as requiring less frequency tuning of the GNR plasmonic resonance and/or the excitation source to switch between different trapping modes. Moreover, it is possible to achieve more quantitative selection of NPs, such as selecting only the NPs with a sufficiently thick coating or a specific type of coating, since the equivalent polarizability of a core/shell NP sensitively depends on the thickness and the permittivity of the shell (i.e., the coating layer).

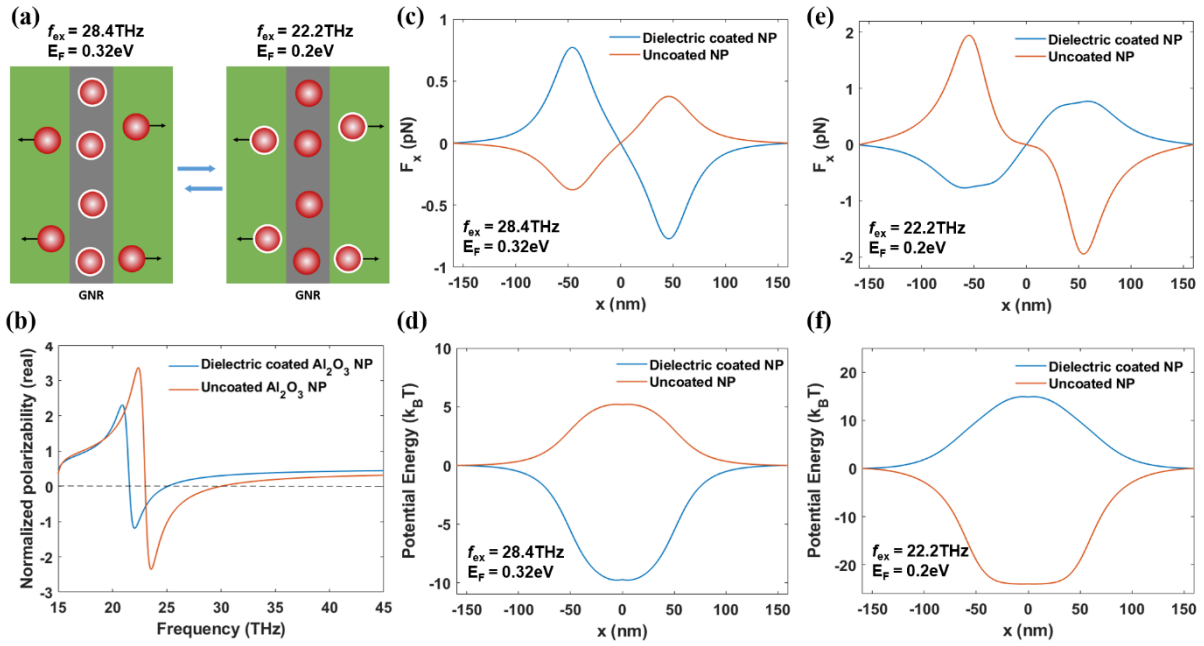


**Figure 5.** NP sorting and fractionating functionality II. (a) Conceptual schematic illustrating the functionality of separating dispersive NPs with and without a thin coating layer by tuning the GNR Fermi energy (and hence plasmonic resonance) and the excitation source frequency. (b) The normalized polarizabilities of  $\text{Al}_2\text{O}_3$  NPs (60 nm diameter) with (blue curve) and without (red curve) a 4 nm thick dielectric coating ( $n=2.5$ ). (c) Calculated x-component ( $F_x$ ) of optical forces on the dielectric-coated (blue curve) and uncoated (red curve)  $\text{Al}_2\text{O}_3$  NPs, and (d) the corresponding potential energy profiles, at the GNR Fermi energy  $E_F=0.32 \text{ eV}$  and the excitation source frequency  $f_{ex}=28.4 \text{ THz}$ . In this operating condition, the coated  $\text{Al}_2\text{O}_3$  NPs are trapped whereas the uncoated  $\text{Al}_2\text{O}_3$  NPs are repelled by the GNR. (e) Calculated x-component ( $F_x$ ) of optical forces on the dielectric-coated (blue curve) and uncoated (red curve)  $\text{Al}_2\text{O}_3$  NPs, and (f) the corresponding potential energy profiles, at the GNR Fermi energy  $E_F=0.2 \text{ eV}$  and the excitation source frequency  $f_{ex}=22.2 \text{ THz}$ . In this operating condition, the uncoated  $\text{Al}_2\text{O}_3$  NPs are trapped whereas the coated  $\text{Al}_2\text{O}_3$  NPs are repelled by the GNR. A moderate excitation source intensity at  $1.5 \text{ mW}/\mu\text{m}^2$  is assumed for calculating the results in this figure.

### 2.3. Discussion

The focus of this work is to systematically investigate the characteristics of tunable bipolar optical forces induced by MIR graphene plasmonic resonances on NPs made of dispersive materials, and conceptually demonstrate versatile optical manipulations beyond optical

trapping which may have various potential applications. Our findings may provide important guidance to future experimental demonstrations. In addition to optical forces, previous experimental studies of optical tweezers and plasmonic tweezers have shown that several other effects caused by light-absorption-induced heating, such as thermophoretic forces and convection in the liquid medium, can also have significant impacts on the trapping and manipulation of target microscopic objects. These heating related effects may compromise the performance of optical trapping and manipulation of target objects accomplished by the optical forces, but may also be utilized to assist the optical trapping and manipulation as well as provide complementary functionalities, as demonstrated previously.<sup>[39-43]</sup> Therefore, the potential heating related effects should be thoroughly taken into account when designing and implementing experimental demonstrations of the system theoretically investigated in this work.

In general, for the system investigated in this work, heat can be produced due to light absorption in the GNR plasmonic resonators, in the materials surrounding the GNRs (e.g., the gate insulator, the encapsulation layer, and the liquid medium), as well as in the target NPs made of dispersive materials. If the goal is to minimize heat generation, materials with low loss in the spectral region of the MIR excitation sources should be used for the gate insulator, the encapsulation layer and the liquid medium. As mentioned previously, organic solvents such as the alkanes are suitable liquid media for this purpose. On the other hand, water is a frequently used liquid medium for many optical trapping and manipulation applications. However, as water has relatively high loss in the MIR region, absorption of the MIR excitation in water is likely significant, which would depend on the specific device structure and experimental setup. One effective approach to reducing the light absorption in water is to employ the plasmonic internal reflection excitation scheme.<sup>[43]</sup> Another beneficial strategy is to optimize the device structure and system configuration, so that the potential effects due to the heating of water can

be utilized to support the optical trapping and manipulation, the details of which is beyond the scope of this work.

Unlike non-dispersive NPs, NPs made of dispersive materials are intrinsically lossy and light absorption in such NPs cannot be avoided. However, as shown in this work and several previous work, the exceedingly high field gradient in the vicinity of MIR graphene plasmonic resonators allows for effective optical trapping and manipulation of NPs with relatively low illumination intensity. As the illumination intensity for the results presented in this work is assumed to be  $1 \text{ mW}/\mu\text{m}^2$ , our simulation shows that the absorbed power in an individual NP (assuming 60 nm diameter) is on the order of  $1 \text{ }\mu\text{W}$  or less, which may lead to a moderate temperature rise of a few degrees Celsius in the surrounding medium (see Supporting Information **Figures S11** and **S12**). By optimizing the device structure, the potential effects stemming from the heating of NPs may also be exploited to assist the optical trapping and manipulation of the NPs.

### 3. Conclusion

In summary, we have systematically studied the characteristics of bipolar optical forces induced by MIR GNR plasmonic tweezers on NPs made of materials with significant permittivity dispersions in the MIR spectral region, which can be described by the Lorentz model. Our study can be applied to a broad range of materials that exhibit strong permittivity dispersions in the MIR region owing to their infrared-active optical phonons, molecular vibrations, or intersubband transitions. As a result of such permittivity dispersions, the polarizability of a NP can exhibit either positive or negative values in different spectral windows, and hence the NP can experience either a trapping or a repulsive force in the vicinity of a GNR supporting a tunable MIR plasmonic resonance. We have shown that by tuning the GNR plasmonic resonance and/or the excitation source frequency, the polarity of the GNR-induced optical force on a dispersive NP can be dynamically reconfigured in real time, which can be utilized for

various applications such as sorting, filtering and fractionating different types of NPs in a mixture. We have further demonstrated two exemplary potential applications, including selectively trapping a particular type of NPs from a mixture of different types, and selectively trapping NPs with (or without) a dielectric coating from a mixture of both coated and uncoated NPs. Our findings presented here demonstrate the unique advantages of employing tunable graphene plasmonic structures to realize optical trapping and manipulation of nanoscale objects in the MIR spectral region, which provide new functionalities that are complementary to those of the existing optical and plasmonic tweezers based on visible and NIR excitation sources, and therefore may enable a wide range of new applications.

#### **4. Methods**

*Simulation and calculation of optical forces:* The electromagnetic field distributions of the investigated structures were simulated using the finite difference time domain method (Ansys Lumerical FDTD). Graphene was modeled as a 2D conductive surface based on the Kubo formula.<sup>[44]</sup> The carrier scattering rate of graphene was set to 1 meV in terms of energy, which corresponds to a carrier scattering time of  $\sim 0.66$  ps. The excitation light is assumed to be a plane wave incident normally on the graphene structures from above. From the simulated electromagnetic field distributions, the optical forces on the NPs were calculated using either the dipole approximation (Equation (1)) or the Maxwell stress tensor method.<sup>[34]</sup> Note that in order to calculate the optical force on a NP with the dipole approximation, the electromagnetic field distribution near the GNR without the NP is simulated and used.

#### **Supporting Information**

Supporting Information is available from the Wiley Online Library or from the author.

#### **Acknowledgements**

This work is supported in part by the National Science Foundation (NSF) (Award No. ECCS-

1847203).

Received: ((will be filled in by the editorial staff))

Revised: ((will be filled in by the editorial staff))

Published online: ((will be filled in by the editorial staff))

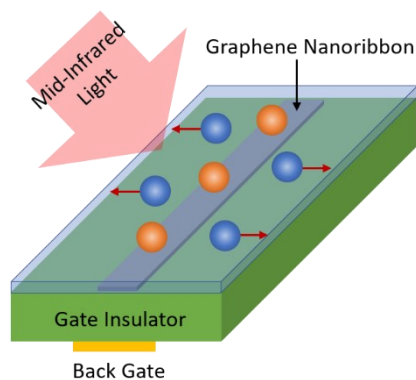
## References

- [1] A. Ashkin, *Phys. Rev. Lett.* **1970**, *24*, 156-159.
- [2] A. Ashkin, J. M. Dziedzic, J. E. Bjorkholm, S. Chu, *Opt. Lett.* **1986**, *11*, 288-290.
- [3] M. E. J. Friese, T. A. Nieminen, N. R. Heckenberg, H. Rubinsztein-Dunlop, *Nature* **1998**, *394*, 348-350.
- [4] M. P. MacDonald, L. Paterson, K. Volke-Sepulveda, J. Arlt, W. Sibbett, K. Dholakia, *Science* **2002**, *296*, 1101-1103.
- [5] A. H. J. Yang, S. D. Moore, B. S. Schmidt, M. Klug, M. Lipson, D. Erickson, *Nature* **2009**, *457*, 71-75.
- [6] S. E. S. Spesyvtseva, K. Dholakia, *ACS Photonics* **2016**, *3*, 719-736.
- [7] Y. Pang, R. Gordon, *Nano Lett.* **2011**, *11*, 3763-3767.
- [8] W. Zhang, L. Huang, C. Santschi, O. J. Martin, *Nano Lett.* **2010**, *10*, 1006-1011.
- [9] Y. Pang, R. Gordon, *Nano Lett.* **2012**, *12*, 402-406.
- [10] D. Yoo, K. L. Gurunatha, H.-K. Choi, D. A. Mohr, C. T. Ertsgaard, R. Gordon, S.-H. Oh, *Nano Lett.* **2018**, *18*, 3637-3642.
- [11] R. A. Jensen, I. C. Huang, O. Chen, J. T. Choy, T. S. Bischof, M. Lončar, M. G. Bawendi, *ACS Photonics* **2016**, *3*, 423-427.
- [12] P. Hansen, Y. Zheng, J. Ryan, L. Hesselink, *Nano Lett.* **2014**, *14*, 2965-2970.
- [13] Y. Zheng, J. Ryan, P. Hansen, Y.-T. Cheng, T.-J. Lu, L. Hesselink, *Nano Lett.* **2014**, *14*, 2971-2976.
- [14] Z. Kang, H. Lu, J. Chen, K. Chen, F. Xu, H.-P. Ho, *Opt. Express* **2014**, *22*, 19567-19572.
- [15] C. Luo, X. Guo, H. Hu, D. Hu, C. Wu, X. Yang, Q. Dai, *Adv. Optical Mater.* **2020**, *8*, 1901416.
- [16] J. Liu, S. Park, D. Nowak, M. Tian, Y. Wu, H. Long, K. Wang, B. Wang, P. Lu, *Laser Photonics Rev.* **2018**, *12*, 1800040.
- [17] L. Wang, H. Wang, M. Wagner, Y. Yan, D. S. Jakob, X. G. Xu, *Sci. Adv.* **2017**, *3*, e1700255.
- [18] L. Ju, B. Geng, J. Horng, C. Girit, M. Martin, Z. Hao, H. A. Bechtel, X. Liang, A. Zettl, Y. R. Shen, F. Wang, *Nat. Nanotechnol.* **2011**, *6*, 630-634.
- [19] H. Yan, X. Li, B. Chandra, G. Tulevski, Y. Wu, M. Freitag, W. Zhu, P. Avouris, F. Xia, *Nat. Nanotechnol.* **2012**, *7*, 330-334.
- [20] V. W. Brar, M. S. Jang, M. Sherrott, J. J. Lopez, H. A. Atwater, *Nano Lett.* **2013**, *13*, 2541-2547.
- [21] Z. Fang, Y. Wang, A. E. Schlather, Z. Liu, P. M. Ajayan, F. J. Garcia de Abajo, P. Nordlander, X. Zhu, N. J. Halas, *Nano Lett.* **2014**, *14*, 299-304.
- [22] P. Q. Liu, F. Valmorra, C. Maissen, J. Faist, *Optica* **2015**, *2*, 135-140.
- [23] B. Zhu, G. Ren, Y. Gao, Y. Yang, M. J. Cryan, S. Jian, *IEEE Photon. Technol. Lett.* **2015**, *27*, 891-894.
- [24] J. Zhang, W. Liu, Z. Zhu, X. Yuan, S. Qin, *Sci. Rep.* **2016**, *6*, 38086.
- [25] M. M. Abbasi, S. Darbari, M. K. Moravvej-Farshi, *Opt. Express* **2019**, *27*, 26648-26660.
- [26] P. Q. Liu, P. Paul, *ACS Photonics* **2020**, *7*, 3456-3466.
- [27] M. Danesh, M. J. Zadeh, T. Zhang, X. Zhang, B. Gu, J.-S. Lu, T. Cao, Z. Liu, A. T. S. Wee, M. Qiu, Q. Bao, S. Maier, C.-W. Qiu, *Laser Photonics Rev.* **2020**, *14*, 2000030.

- [28] M. P. MacDonald, G. C. Spalding, K. Dholakia, *Nature* **2003**, *426*, 421-424.
- [29] M. M. Wang, E. Tu, D. E. Raymond, J. M. Yang, H. Zhang, N. Hagen, B. Dees, E. M. Mercer, A. H. Forster, I. Kariv, P. J. Marchand, W. F. Butler, *Nat. Biotechn.* **2005**, *23*, 83-87.
- [30] B. J. Roxworthy, K. D. Ko, A. Kumar, K. H. Fung, E. K. C. Chow, G. L. Liu, N. X. Fang, K. C. Toussaint Jr., *Nano Lett.* **2012**, *12*, 796-801.
- [31] M. Ploschner, T. Cizmar, M. Mazilu, A. Di Falco, K. Dholakia, *Nano Lett.* **2012**, *12*, 1923-1927.
- [32] F. Nan, Z. Yan, *Nano Lett.* **2018**, *18*, 4500-4505.
- [33] Y. Shi, H. Zhao, L. K. Chin, Y. Zhang, P. H. Yap, W. Ser, C.-W. Qiu, A. Q. Liu, *Nano Lett.* **2020**, *20*, 5193-5200.
- [34] L. Novotny, B. Hecht, *Principles of Nano-Optics*, 2<sup>nd</sup> edition, Cambridge University Press, Cambridge, UK **2012**, Ch. 14.
- [35] B. T. Draine, *Astrophys. J.* **1988**, *333*, 848-872.
- [36] J. R. Arias-Gonzalez, M. Nieto-Vesperinas, *J. Opt. Soc. Am. A* **2003**, *20*, 1201-1209.
- [37] P. C. Chaumet, M. Nieto-Vesperinas, *Phys. Rev. B* **2000**, *62*, 11185-11191.
- [38] C. Y. Yang, U. Lei, *J. Appl. Phys.* **2007**, *102*, 094702.
- [39] T. Shoji, M. Shibata, N. Kitamura, F. Nagasawa, M. Takase, K. Murakoshi, A. Nobuhiro, Y. Mizumoto, H. Ishihara, Y. Tsuboi, *J. Phys. Chem. C* **2013**, *117*, 2500-2506.
- [40] B. J. Roxworthy, A. M. Bhuiya, S. P. Vanka, K. C. Toussaint, *Nat. Commun.* **2014**, *5*, 3173.
- [41] J. C. Ndukaiife, A. V. Kildishev, A. G. A. Nnanna, V. M. Shalaev, S. T. Wereley, A. Boltasseva, *Nat. Nanotechnol.* **2016**, *11*, 53-59.
- [42] L. Lin, X. Peng, X. Wei, Z. Mao, C. Xie, Y. Zheng, *ACS Nano* **2017**, *11*, 3147-3154.
- [43] R. Adato, H. Altug, *Nat. Commun.* **2013**, *4*, 2154.
- [44] G. W. Hanson, *J. Appl. Phys.* **2008**, *103*, 064302.

**Table of Content Figure****Dynamically Reconfigurable Bipolar Optical Gradient Force Induced by Mid-Infrared Graphene Plasmonic Tweezers for Sorting Dispersive Nanoscale Objects**

Puspita Paul, Peter Q. Liu\*



This paper demonstrates that mid-infrared graphene plasmonic tweezers can exert dynamically reconfigurable bipolar optical gradient forces on nanoscale objects made of dispersive materials. Such reconfigurable bipolar optical forces can be highly useful for a broad range of applications such as sorting, filtering and fractionating different types of nanoscale objects in a mixture.